Joint International Topical Meeting on Mathematics & Computation and Supercomputing in Nuclear Applications (M&C + SNA 2007)
Monterey, California, April 15-19, 2007, on CD-ROM, American Nuclear Society, LaGrange Park, IL (2007)

EVALUATION OF BWR CORE ATTRIBUTES UNCERTAINTIES DUE TO MULTI-GROUP CROSS-SECTION UNCERTAINTIES

Matthew A. Jessee, Hany S. Abdel-Khalik, and Paul J. Turinsky
Department of Nuclear Engineering
North Carolina State University
P.O. Box 7909
Raleigh, NC 27695-7909
Email: majessee@ncsu.edu, abdelkhalik@ncsu.edu, and turinsky@ncsu.edu

ABSTRACT

This paper outlines the current work on the propagation of multi-group cross-section uncertainties to BWR core attributes uncertainties. The ORNL PUFF-III code propagates the ENDF point-wise cross-section uncertainties to the multi-group level. Our work propagates the multi-group cross-section uncertainties through the subsequent nuclear calculations in a computationally efficient manner. This includes the propagation of multi-group uncertainties through lattice physics codes to generate lattice-averaged few-group cross-section uncertainties. This is followed by reactor calculations to propagate few-group cross-section uncertainties to uncertainties in evaluated core attributes, e.g. core reactivity, nodal power, and reactivity coefficients. In this work, all cross-section uncertainties are assumed to follow normal Gaussian distributions, and only the first and second moments of the uncertainty distributions, i.e. the means and covariances, are propagated through the calculations.
The critical issue in this approach is the computational burden of the sensitivity analysis-type calculations required for the uncertainty analysis. This paper outlines a direct method of propagating cross-sections uncertainties through each computational model in an accurate and computationally efficient manner based on the singular value decomposition of the cross-sections covariance matrices. Core attributes' uncertainties are determined for two different evaluations of the multi-group uncertainty libraries provided in the ORNL SCALE code package. The core attributes' uncertainties are then used to adjust few-group cross-sections to improve the agreement between two different core simulator models by a process referred to as Adaptive Simulation. Posterior few-group cross-section covariance matrices and core attributes covariance matrices are calculated along with the adapted solution.

Key Words: Cross-section Uncertainty Analysis, Singular Value Decomposition

1. INTRODUCTION

Understanding uncertainties in key reactor core attributes associated with BWR core simulation is important in regard to introducing appropriate design margins, and deciding where additional efforts should be undertaken to reduce uncertainties. Uncertainties in core simulation predictions occur due to input data uncertainties, modeling errors, and numerical approximations. Input data to a typical core simulator primarily include the lattice-averaged few-group cross-sections, and the various coefficients that appear in many of the empirical correlations used in reactor calculations, e.g. heat transfer coefficients, void-quality correlations parameters, etc. Previous

work by Abdel-Khalik and Turinsky has shown that cross-sections uncertainties play a significant role in the core attributes uncertainties for a BWR core loaded with LEU fuel [1]. This paper continues investigation into cross-section uncertainty propagation using their developed Efficient Subspace Method (ESM).

ESM is used to perform sensitivity and uncertainty analysis for applications with large input/output (I/O) streams while minimizing the number of required model modifications and evaluations [2]. ESM is based on matrix-revealing decompositions, e.g. singular value decomposition (SVD), which identifies the effective number of degrees of freedom (DOFs), i.e. informational content, of the I/O streams – that is the number of independent pieces of information of potential importance that are transferred through the computational models. In previous work, ESM has shown that the sensitivity matrix of a typical BWR core simulator has a very small effective rank, i.e. small number of potentially important DOFs, compared to the matrix dimensions, a sensitivity matrix which relates changes in calculated responses to changes in input data; it has $m \times n$ entries, where m is the number of calculated responses and n number of input data. This implies significant contraction of the information carried by the input data and high degree of induced correlations among the calculated responses. ESM takes advantage of this situation by limiting the sensitivity and uncertainty analyses to the potentially important independent information that is transferred through the computational model. In this approach, accurate low-rank approximations of the sensitivity and uncertainty matrices can be created directly without ever forming the full matrices, thus reducing the computational and storage burdens to a minimum. For this work, the SVD of the multi-group covariance library is shown to favorably limit the required number of lattice physics calculations and core simulations needed for both uncertainty propagation and adaptive simulation.

Section 2 describes how ESM is used for uncertainty propagation, adaptive simulation, and posterior uncertainty estimation by SVD. The multi-group cross-section covariance matrix is propagated through the lattice physics calculations to calculate the lattice-averaged few-group cross-section covariance matrix. This covariance matrix is propagated through the core simulator to determine uncertainty in BWR core attributes. The covariance matrices and model sensitivities are then used to improve agreement between two different core simulator models with one simulator assumed to represent real plant data and the other an existing design basis core simulator. The adapted simulator is used to update the cross-sections and core attributes covariance matrices, often referred to as posteriori covariance matrices. Section 3 provides results and analysis of these calculations followed by conclusions in section 4.

2. METHODS

The following notation will be used throughout the paper: $\overline{\overline{\mathbf{C}}}$ denotes a matrix, with $[\overline{\overline{\mathbf{C}}}]_{ij}$ being the i-th row and j-th column entry; and $[\overline{\overline{\mathbf{C}}}]_{i*}$ the i-th row, and $[\overline{\overline{\mathbf{C}}}]_{*j}$ the j-th column. $\overline{\mathbf{x}}$ denotes a vector with the k-th entry, $\{\overline{\mathbf{x}}\}_k$. Finally, $\mathbf{\Theta}(\cdot)$ represents a nonlinear operator.

In order to propagate first and second order moments of input data uncertainties through a computational model to the calculated model responses, one needs: a) the covariance matrix of

the input data, and b) the sensitivity matrix characterizing the change in calculated responses with respect to the change in input data [3]. In our work, the computational model is represented by the lattice physics and the core simulation calculations. Let $\boldsymbol{\Theta}$ denote the computational model, such that:

$$\bar{\mathbf{y}} = \boldsymbol{\Theta}(\bar{\mathbf{x}}) \tag{1}$$

where $\bar{\mathbf{x}}$ is an *n*-th dimensional column vector of input parameters, $\bar{\mathbf{y}}$ is an *m*-th dimensional column vector of output responses, and the sensitivity (or Jacobian) matrix $\bar{\bar{\boldsymbol{\Theta}}}$ of the computational model can be defined as:

$$[\bar{\bar{\boldsymbol{\Theta}}}]_{ij} = \left.\frac{\partial\{\bar{\mathbf{y}}\}_i}{\partial\{\bar{\mathbf{x}}\}_j}\right|_{\bar{\mathbf{x}}_0} \tag{2}$$

for $i=1,\ldots,m$, and $j=1,\ldots,n$, where all partial derivatives are evaluated at a reference input $\bar{\mathbf{x}}_0$ producing output $\bar{\mathbf{y}}_0 = \boldsymbol{\Theta}(\bar{\mathbf{x}}_0)$. Given $\bar{\bar{\mathbf{C}}}_x$ the input parameters covariance matrix, the second order moment of output responses' uncertainties may be characterized by:

$$\bar{\bar{\mathbf{C}}}_y = \bar{\bar{\boldsymbol{\Theta}}}\bar{\bar{\mathbf{C}}}_x\bar{\bar{\boldsymbol{\Theta}}}^{\mathbf{T}} \tag{3}$$

where $\bar{\bar{\mathbf{C}}}_y$ is the output responses covariance matrix.[1] In conventional uncertainty analysis approaches, $\bar{\bar{\mathbf{C}}}_y$ is directly calculated by the triple matrix product in Eq. 3, where $\bar{\bar{\boldsymbol{\Theta}}}$ is calculated using forward or adjoint methods. The forward method requires $n + 1$ forward calculations where $[\bar{\bar{\boldsymbol{\Theta}}}]_{*j}$ is:

$$[\bar{\bar{\boldsymbol{\Theta}}}]_{*j} = \frac{\boldsymbol{\Theta}(\bar{\mathbf{x}}_0 + \varepsilon\,\bar{\mathbf{e}}_j) - \bar{\mathbf{y}}_0}{\varepsilon} \tag{4}$$

and ε is a scaling factor chosen to produce a linear response for $\boldsymbol{\Theta}$ near $\bar{\mathbf{x}}_0$. Likewise, adjoint methods require $m + 1$ adjoint calculations to calculate $\bar{\bar{\boldsymbol{\Theta}}}$.

2.1. Uncertainty Propagation

For our work, the effective rank of the input parameters covariance matrix $\bar{\bar{\mathbf{C}}}_x$ is found to be very small compared to the total number of input parameters. This implies that only a small subset of input data has independent uncertainty information. The selected DOFs were based on

[1] For our work, relative sensitivity and relative covariance matrices were used. Absolute sensitivity and covariance matrices are presented to simplify notations.

the SVD of $\overline{\overline{\mathbf{C}}}_x$ and used to calculate $\overline{\overline{\mathbf{C}}}_y$ in the following equivalent formulation using only r + 1 forward model evaluations. Note that r is selected by ordering the singular values from high to low, and then selecting r such that the r +1 singular value is several orders of magnitude smaller than the 1st singular value. In what follows, it will be assumed usage of the effective rank introduces error that can be ignored, so effective rank and rank can be considered equivalent. Note that the sensitivity matrix of the computational model, also found to be of low rank, is expected to decrease the number of DOFs propagated through the lattice physics even further, however with very low r, the required number of forward model evaluations is affordable. Now, express the compact SVD of $\overline{\overline{\mathbf{C}}}_x$ as:

$$\overline{\overline{\mathbf{C}}}_x = \overline{\overline{\mathbf{U}}}_x \overline{\overline{\mathbf{\Sigma}}}_x \overline{\overline{\mathbf{U}}}_x^T \tag{5}$$

where $\overline{\overline{\mathbf{U}}}_x \in R^{n \times r}$ with r orthogonal columns that span the range of $\overline{\overline{\mathbf{C}}}_x$, and $\overline{\overline{\mathbf{\Sigma}}}_x \in R^{r \times r}$ is a diagonal matrix of singular values. Substituting for $\overline{\overline{\mathbf{C}}}_x$ in Eq. 3, $\overline{\overline{\mathbf{C}}}_y$ reduces to:

$$\overline{\overline{\mathbf{C}}}_y = \overline{\overline{\mathbf{R}}}_y \overline{\overline{\mathbf{\Sigma}}}_x \overline{\overline{\mathbf{R}}}_y^T \tag{6}$$

where $\overline{\overline{\mathbf{R}}}_y = \overline{\overline{\mathbf{\Theta}}}\,\overline{\overline{\mathbf{U}}}_x \in R^{m \times r}$ is defined as the response matrix whose j-th column represents the action of the sensitivity matrix along the j-th column of $\overline{\overline{\mathbf{U}}}_x$, i.e. the directional derivative along the j-th column of $\overline{\overline{\mathbf{U}}}_x$, whose matrix-free [4] forward difference approximation is:

$$[\overline{\overline{\mathbf{R}}}_y]_{*j} = \overline{\overline{\mathbf{\Theta}}}[\overline{\overline{\mathbf{U}}}_x]_{*j} = \frac{\mathbf{\Theta}(\overline{\mathbf{x}}_0 + \varepsilon[\overline{\overline{\mathbf{U}}}_x]_{*j}) - \overline{\mathbf{y}}_0}{\varepsilon} \tag{7}$$

where ε is again a scaling factor chosen to produce a linear response for $\mathbf{\Theta}$ near $\overline{\mathbf{x}}_0$. The columns of $\overline{\overline{\mathbf{U}}}_x$ are referred to as the principal directions of $\overline{\overline{\mathbf{C}}}_x$.

Eq. 6 is used to determine the lattice-averaged few-group cross-section covariance matrix $\overline{\overline{\mathbf{C}}}_{FG}$ from the multi-group covariance matrix $\overline{\overline{\mathbf{C}}}_{MG}$:

$$\overline{\overline{\mathbf{C}}}_{FG} = \overline{\overline{\mathbf{R}}}_l \overline{\overline{\mathbf{\Sigma}}}_{MG} \overline{\overline{\mathbf{R}}}_l^T \tag{8}$$

where $\overline{\overline{\mathbf{R}}}_l = \overline{\overline{\mathbf{\Theta}}}_l \overline{\overline{\mathbf{U}}}_{FG}$ is the lattice physics response matrix with sensitivity matrix $\overline{\overline{\mathbf{\Theta}}}_l$. The multi-group covariance matrix is constructed using the multi-group covariance libraries (44GROUPV5COV and 44GROUPANLCOV) provided in the SCALE 5.0 package [5]. These libraries were generated by the multi-group preparation code PUFF-III [6], which processes the

ENDF/V point-wise covariance data. Likewise, the core attributes covariance matrix $\overline{\overline{\mathbf{C}}}_{CA}$ can be calculated as:

$$\overline{\overline{\mathbf{C}}}_{CA} = \overline{\overline{\boldsymbol{\Theta}}}_c \overline{\overline{\mathbf{R}}}_l \overline{\overline{\boldsymbol{\Sigma}}}_{MG} \overline{\overline{\mathbf{R}}}_l^T \overline{\overline{\boldsymbol{\Theta}}}_c^T \tag{9}$$

where $\overline{\overline{\boldsymbol{\Theta}}}_c$ is the core simulator sensitivity matrix. The response matrix representation is formed by the SVD of $\overline{\overline{\mathbf{R}}}_l \overline{\overline{\boldsymbol{\Sigma}}}_{MG}^{1/2} = \overline{\overline{\mathbf{U}}}_{FG} \overline{\overline{\boldsymbol{\Sigma}}}_{FG}^{1/2} \overline{\overline{\boldsymbol{\Psi}}}^T$. Eq. 9 becomes:

$$\begin{aligned} \overline{\overline{\mathbf{C}}}_{CA} &= \overline{\overline{\boldsymbol{\Theta}}}_c \overline{\overline{\mathbf{U}}}_{FG} \overline{\overline{\boldsymbol{\Sigma}}}_{FG}^{1/2} \overline{\overline{\boldsymbol{\Psi}}}^T \overline{\overline{\boldsymbol{\Psi}}} \overline{\overline{\boldsymbol{\Sigma}}}_{FG}^{1/2} \overline{\overline{\mathbf{U}}}_{FG}^T \overline{\overline{\boldsymbol{\Theta}}}_c^T \\ &= \overline{\overline{\boldsymbol{\Theta}}}_c \overline{\overline{\mathbf{U}}}_{FG} \overline{\overline{\boldsymbol{\Sigma}}}_{FG} \overline{\overline{\mathbf{U}}}_{FG}^T \overline{\overline{\boldsymbol{\Theta}}}_c^T \\ &= \overline{\overline{\mathbf{R}}}_c \overline{\overline{\boldsymbol{\Sigma}}}_{FG} \overline{\overline{\mathbf{R}}}_c^T \end{aligned} \tag{10}$$

with $\overline{\overline{\mathbf{R}}}_c = \overline{\overline{\boldsymbol{\Theta}}}_c \overline{\overline{\mathbf{U}}}_{FG}$ is the core simulator response matrix.

For our problem, the I/O streams are very large: a) ~10^3 multi-group cross-sections input to the lattice physics code, b) ~10^6 lattice-averaged few-group cross-sections generated by ~10^2 runs of the lattice physics code to functionalize cross-sections in terms of various historical and instantaneous core conditions, e.g. exposure, void, fuel and moderator temperature changes, and control rod insertion, etc., and c) ~10^5 core attributes (k_{eff}'s, nodal powers, thermal margins calculated at various points during depletion). Using standard sensitivity analyses would require too many code runs to render a practical approach to uncertainty evaluation. For example, the forward approach would require ~10^5 and 10^6 lattice physics and core simulator runs, respectively, in order to evaluate the full lattice physics' and core simulator's sensitivity matrices, i.e. $\overline{\overline{\boldsymbol{\Theta}}}_l$ and $\overline{\overline{\boldsymbol{\Theta}}}_c$. An adjoint sensitivity analysis would require ~10^6 and 10^5 lattice physics and simulators runs, respectively, where the codes have to be run in an adjoint mode which often requires extensive coding effort to implement. In this work, we have utilized an ESM-based sensitivity analysis. This approach evaluates the sensitivity information associated with the effective DOFs only, i.e. the information that is transferred through the lattice physics and core simulators codes. To identify the effective DOFs for an uncertainty analysis application[2], we recognize that the rank of $\overline{\overline{\mathbf{C}}}_{MG}$ is only 10^2 due to the high degree of correlation amongst the multi-group cross-sections. This implies that the effective number of DOFs characterizing the few-group cross-sections uncertainties cannot exceed 10^2. Once identified, one needs to run the core simulator ~10^2 times only in order to propagate uncertainties to core attributes. Since we are relying on forward calculations only, one, in general, would need to run the lattice physics code ~10^2x10^2 times to identify the ~10^2 effective DOFs. For this work, the lattice physics response matrix was generated for one representative lattice/void configuration

[2] The effective DOFs will vary depending on the application. For example, in an uncertainty analysis, one is only interested in propagating uncertainty information for input data that have relatively high-to-moderate uncertainties and high-to-moderate sensitivities. All DOF with zero uncertainties are discarded from the analysis even if they have strong sensitivities since they do not contribute to the propagated uncertainties.

and these results were then fully correlated to all lattice/void configurations, reducing the number of lattice physics computations to 10^2. Previous work suggests that different lattice/void configurations have different correlations and that in general all lattice/void configurations should be modeled explicitly [2]. A current research area includes developing a fast, accurate low-order lattice physics model that calculates these correlations along with using ESM to determine an accurate low-rank approximation to $\overline{\overline{\mathbf{\Theta}}}_l$. The singular value decomposition of $\overline{\overline{\mathbf{C}}}_{FG}$ revealed a decrease in the effective number of DOFs through the lattice physics model; as expected only ~10^2 core simulation runs were required to calculate $\overline{\overline{\mathbf{C}}}_{CA}$.

2.2. Adaptive Simulation

Adaptive simulation is an inverse problem that minimizes the residual between a set of measurements and model predictions by adjusting model input data [2]. For BWR simulation, we are interested in adjusting $n = 10^6$ lattice-averaged few-group cross-sections to minimize the discrepancies between $m = 10^5$ measured and predicted core attributes. Ultimately, the measurements will be based on real plant data, however in this work a virtual approach has been adopted, where one core simulator's predictions are assumed to represent real plant data while another simulator is taken to represent an existing design basis core simulator. With the large size of input and output data of a typical core simulator, it is apparent that a prohibitive number of forward and/or adjoint simulator runs will be required to explicitly calculate $\overline{\overline{\mathbf{\Theta}}}_c$. This is necessary for any Gradient-based nonlinear least-squares solver, e.g. Newton or quasi-Newton-type methods [4]. As presented, the adaption problem is undetermined since the number of equations m is less than the number of unknowns n. Mathematically, this problem is referred to as being ill-posed [7], where one cannot obtain a unique solution. In addition, it has been demonstrated that any noise inherent in the measurements can lead to an unreliable adaption. To re-cast an ill-posed problem into a well-posed one, a regularization approach is often used, specifically Tikhonov Regularization has been adopted in our work [8]. In addition, the few-group cross-sections adjustments have also been constrained to a subspace spanned by the singular vectors of the covariance matrix $\overline{\overline{\mathbf{C}}}_{FG}$. This is done to ensure statistical consistency of the adjusted cross-section. As pointed out earlier, the rank of $\overline{\overline{\mathbf{C}}}_{FG}$ is only of the order of 10^2, implying that only 10^2 core simulator runs are required to create the core simulator response matrix $\overline{\overline{\mathbf{R}}}_c$.

In our implementation, the Tikhonov-regularized objective function is defined as:

$$Obj(\overline{\mathbf{z}}) = \left\| \overline{\mathbf{y}}_{CA(m)} - \mathbf{\Theta}_c(\overline{\mathbf{x}}_{FG}) \right\|^2_{\overline{\overline{\mathbf{C}}}^{-1}_{CA(m)}} + \alpha^2 \left\| \overline{\mathbf{x}}_{FG} - \overline{\mathbf{x}}_{FGo} \right\|^2_{\overline{\overline{\mathbf{C}}}^{+}_{FG}} \tag{11}$$

$$\text{subject to } \overline{\mathbf{x}}_{FG} - \overline{\mathbf{x}}_{FGo} = \overline{\overline{\mathbf{U}}}_{FG}\overline{\mathbf{z}} \tag{12}$$

where the first term, known as the misfit term, is the distance between a measured $\overline{\mathbf{y}}_{CA(m)} \in R^m$ and a predicted $\overline{\mathbf{y}}_{CA} = \mathbf{\Theta}_c(\overline{\mathbf{x}}_{FG})$ set of core attributes for some set of lattice-averaged few-group cross-sections $\overline{\mathbf{x}}_{FG} \in R^n$. The misfit norm is weighted by the inverse of the measured core

attributes covariance matrix $\overline{\overline{\mathbf{C}}}_{CA(m)}$. The second term, known as the regularization term, is the distance between $\bar{\mathbf{x}}_{FG}$ and the priori values $\bar{\mathbf{x}}_{FGo}$ where the norm is weighted by the Moore-Penrose pseudo inverse for $\overline{\overline{\mathbf{C}}}_{\boldsymbol{FG}}$ ($\overline{\overline{\mathbf{C}}}_{FG}^{+} = \overline{\overline{\mathbf{U}}}_{FG}\overline{\overline{\mathbf{\Sigma}}}_{FG}^{-1}\overline{\overline{\mathbf{U}}}_{FG}^{T}$) – note that $\overline{\overline{\mathbf{C}}}_{\boldsymbol{FG}}$ is singular. The constraint defined by Eq. 12 ensures that the few-group cross-section adjustments will belong to the subspace spanned by the columns of the matrix $\overline{\overline{\mathbf{U}}}_{FG}$, where $\bar{\mathbf{z}} \in R^{r}$ represents the component, e.g. expansion coefficients, of the cross-sections adjustment vector $\bar{\mathbf{x}}_{FG} - \bar{\mathbf{x}}_{FGo}$ along the columns of the matrix $\overline{\overline{\mathbf{U}}}_{FG}$. The regularization parameter α is used to control the magnitude of the cross-section adjustments, and is experimentally determined by "trial and error" based on the characteristic 'L-curve' [9].

Eq. 11 and Eq. 12 can be reduced to the following linear least squares minimization problem:

$$Obj(\bar{\mathbf{z}}) = \| \bar{\mathbf{b}} - \overline{\overline{\mathbf{A}}}\bar{\mathbf{z}} \|_2^2 \tag{13}$$

where $\overline{\overline{\mathbf{A}}} \in R^{m+r \times r}$ is of full column rank such that Eq. 13 can be solved by orthogonal decomposition or direct solution to the normal equation, i.e. $\bar{\tilde{\mathbf{z}}} = (\overline{\overline{\mathbf{A}}}^{T}\overline{\overline{\mathbf{A}}})^{-1}\overline{\overline{\mathbf{A}}}^{T}\bar{\mathbf{b}}$. To show that, starting with the SVD of $\overline{\overline{\mathbf{C}}}_{CA(m)}$, one can re-write Eq. 11 using the following 2-norm expression:

$$\begin{aligned} Obj(\bar{\mathbf{z}}) &= \| \overline{\overline{\mathbf{\Sigma}}}_{CA(m)}^{-1/2}\overline{\overline{\mathbf{U}}}_{CA(m)}^{T}(\bar{\mathbf{y}}_{CA(m)} - \mathbf{\Theta}_c(\bar{\mathbf{x}}_{FG})) \|_2^2 + \alpha^2 \| \overline{\overline{\mathbf{\Sigma}}}_{FG}^{-1/2}\overline{\overline{\mathbf{U}}}_{FG}^{T}(\bar{\mathbf{x}}_{FG} - \bar{\mathbf{x}}_{FGo}) \|_2^2 \\ &= \| \overline{\overline{\mathbf{\Sigma}}}_{CA(m)}^{-1/2}\overline{\overline{\mathbf{U}}}_{CA(m)}^{T}(\bar{\mathbf{y}}_{CA(m)} - \mathbf{\Theta}_c(\bar{\mathbf{x}}_{FG})) \|_2^2 + \alpha^2 \| \overline{\overline{\mathbf{\Sigma}}}_{FG}^{-1/2}\bar{\mathbf{z}} \|_2^2 \end{aligned} \tag{14}$$

where $\bar{\mathbf{z}} = \overline{\overline{\mathbf{U}}}_{FG}^{T}\left(\bar{\mathbf{x}}_{FG} - \bar{\mathbf{x}}_{FGo}\right)$ is substituted into the regularization term from Eq. 12. The core simulator model can be linearized about $\bar{\mathbf{x}}_{FGo}$ such that:

$$\bar{\mathbf{y}}_{CA} = \mathbf{\Theta}_c(\bar{\mathbf{x}}_{FG}) \approx \bar{\mathbf{y}}_{CAo} + \overline{\overline{\mathbf{\Theta}}}_c\left(\bar{\mathbf{x}}_{FG} - \bar{\mathbf{x}}_{FGo}\right) = \bar{\mathbf{y}}_{CAo} + \overline{\overline{\mathbf{\Theta}}}_c\overline{\overline{\mathbf{U}}}_{FG}\bar{\mathbf{z}} = \bar{\mathbf{y}}_{CAo} + \overline{\overline{\mathbf{R}}}_c\bar{\mathbf{z}} \tag{15}$$

where $\bar{\mathbf{y}}_{CAo} \equiv \mathbf{\Theta}_c(\bar{\mathbf{x}}_{FGo})$ and $\overline{\overline{\mathbf{R}}}_c$ is the core simulator response matrix. Substituting Eq. 15 into Eq. 14 yields:

$$\| \overline{\overline{\mathbf{\Sigma}}}_{CA(m)}^{-1/2}\overline{\overline{\mathbf{U}}}_{CA(m)}^{T}(\bar{\mathbf{y}}_{CA(m)} - \bar{\mathbf{y}}_{CAo} - \overline{\overline{\mathbf{R}}}_c\bar{\mathbf{z}}) \|_2^2 + \alpha^2 \| \overline{\overline{\mathbf{\Sigma}}}_{FG}^{-1/2}\bar{\mathbf{z}} \|_2^2 = \| \bar{\mathbf{b}} - \overline{\overline{\mathbf{A}}}\bar{\mathbf{z}} \|_2^2 \tag{16}$$

where

$$\overline{\overline{\mathbf{A}}} \in R^{m+r\times r} = \begin{bmatrix} \overline{\overline{\boldsymbol{\Sigma}}}_{CA(m)}^{-1/2}\,\overline{\overline{\mathbf{U}}}_{CA(m)}^{T}\,\overline{\overline{\mathbf{R}}}_c \\ \alpha\overline{\overline{\boldsymbol{\Sigma}}}_{FG}^{-1/2} \end{bmatrix}, \text{ and } \overline{\mathbf{b}} \in R^{m+r} = \begin{bmatrix} \overline{\overline{\boldsymbol{\Sigma}}}_{CA(m)}^{-1/2}\,\overline{\overline{\mathbf{U}}}_{CA(m)}^{T}\left(\overline{\mathbf{y}}_{CA(m)} - \overline{\mathbf{y}}_{CAo}\right) \\ \overline{0} \end{bmatrix} \tag{17}$$

The minimizer of Eq. 16, denoted as $\overline{\tilde{\mathbf{z}}}$, is the least-squares solution to the following equation:

$$\overline{\overline{\mathbf{A}}}\overline{\tilde{\mathbf{z}}} = \overline{\mathbf{b}} \tag{18}$$

Instead of using the normal equations to calculate $\overline{\tilde{\mathbf{z}}}$, i.e. $\overline{\tilde{\mathbf{z}}} = (\overline{\overline{\mathbf{A}}}^{T}\overline{\overline{\mathbf{A}}})^{-1}\overline{\overline{\mathbf{A}}}^{T}\overline{\mathbf{b}}$, we use an SVD-based approach to avoid squaring the condition number of the matrix $\overline{\overline{\mathbf{A}}}$. Calculating the SVD of the top block of $\overline{\overline{\mathbf{A}}}$ such as:

$$\overline{\overline{\mathbf{A}}} = \begin{bmatrix} \overline{\overline{\boldsymbol{\Sigma}}}_{CA(m)}^{-1/2}\,\overline{\overline{\mathbf{U}}}_{CA(m)}^{T}\,\overline{\overline{\mathbf{R}}}_c \\ \alpha\overline{\overline{\boldsymbol{\Sigma}}}_{FG}^{-1/2} \end{bmatrix} = \begin{bmatrix} \overline{\overline{\mathbf{U}}}_A\,\overline{\overline{\boldsymbol{\Sigma}}}_A\,\overline{\overline{\mathbf{V}}}_A^{T} \\ \alpha\overline{\overline{\boldsymbol{\Sigma}}}_{FG}^{-1/2} \end{bmatrix} \tag{19}$$

The minimizer $\overline{\tilde{\mathbf{z}}}$ can then be given by:

$$\overline{\tilde{\mathbf{z}}} = (\overline{\overline{\mathbf{V}}}_A\overline{\overline{\boldsymbol{\Sigma}}}_A^{2}\overline{\overline{V}}^{T} + \alpha^2\overline{\overline{\boldsymbol{\Sigma}}}_{FG}^{-1})^{-1}\overline{\overline{\mathbf{V}}}_A\overline{\overline{\boldsymbol{\Sigma}}}_A\overline{\overline{\mathbf{U}}}_A^{T}\overline{\mathbf{b}} \tag{20}$$

The adaptive simulation algorithm may be outlined as follows:

Given: $\overline{\overline{\mathbf{U}}}_{FG}$, $\overline{\overline{\boldsymbol{\Sigma}}}_{FG}$ from the SVD of the few-group covariance matrix, $\overline{\mathbf{y}}_{CA(m)}$ the measured core attributes, and $\overline{\overline{\mathbf{C}}}_{CA(m)}$ the covariance matrix of measured core attributes – often a diagonal matrix.

1. Calculate $\overline{\mathbf{y}}_{CAo} = \boldsymbol{\Theta}_c\left(\overline{\mathbf{x}}_{FGo}\right)$
2. Run the core simulator *r* times in a forward manner to calculate $\overline{\overline{\mathbf{R}}}_c$ (Eq. 7).
3. Calculate the SVD of $\overline{\overline{\mathbf{C}}}_{CA(m)}$ if unknown.
4. Construct $\overline{\overline{\mathbf{A}}}$ and $\overline{\mathbf{b}}$ from Eq. 17.
5. Solve for $\overline{\tilde{\mathbf{z}}}$ from Eq. 20.
6. Calculate the adapted few-group cross-sections $\overline{\tilde{\mathbf{x}}}_{FG} = \overline{\mathbf{x}}_{FG0} + \overline{\overline{\mathbf{U}}}_{FG}\overline{\tilde{\mathbf{z}}}$.
7. Calculate the adapted core attributes $\overline{\tilde{\mathbf{y}}}_{CA} = \boldsymbol{\Theta}_c\left(\overline{\tilde{\mathbf{x}}}_{FG}\right)$.

In our implementation, it is assumed that the uncertainties for both the input data (i.e. few-group cross-sections) and measured output data (i.e. core attributes) follow Gaussian probability distributions. This is likely an acceptable assumption for the input data - only the first and second moments (i.e. means and variances) of the cross-sections are available in the evaluated nuclear data files. For the measured core attributes, we assume that the measured signals have been corrected for calibration errors prior to being incorporated into the adaption. With these

assumptions, one can show the measured core attributes and the posteriori (adjusted) cross-sections will indeed follow Gaussian distributions if the lattice physics and core simulator codes are behaving linearly within the range of the cross-section adjustments [10]. Numerical experiments have revealed that the change in few-group cross-sections is directly proportional to the change in multi-group cross-sections up to perturbations of ~1-4 standard deviations. This assures that any adjusted data within the tails of the prior distributions will still produce a linear response. The following condition is utilized to assess the linearity of the lattice physics and the core simulator model:

$$\boldsymbol{\Theta}(\bar{\mathbf{x}}_0 + \bar{\bar{\mathbf{X}}}\bar{\boldsymbol{\beta}}) - \boldsymbol{\Theta}(\bar{\mathbf{x}}_0) \approx \sum_{i=1}^{k} [\boldsymbol{\Theta}(\bar{\mathbf{x}}_0 + \{\bar{\boldsymbol{\beta}}\}_i [\bar{\bar{\mathbf{X}}}]_{*i}) - \boldsymbol{\Theta}(\bar{\mathbf{x}}_0)] \tag{21}$$

where $\bar{\boldsymbol{\beta}} \in R^k$ is a vector of perturbation weights, *k* is the number of perturbations, and the columns of $\bar{\bar{\mathbf{X}}} \in R^{n \times k}$ represent random directions along which the input data are perturbed. Eq. 18 was tested for various choices of *k*, $\bar{\boldsymbol{\beta}}$, and $\bar{\bar{\mathbf{X}}}$ such that the magnitudes of the perturbed cross-sections vary from 0 to 4 standard deviations.

2.2. Posterior Covariance Matrices

The posterior uncertainties associated with the solution to an inverse problem are just as important as the posterior solution (i.e. adapted solution). Posterior uncertainty analysis updates the input data uncertainties, i.e. our confidence in their reported values, based on the measured core attributes. Essentially, adaptive simulation utilizes data from additional experiments to increase our confidence about the reported input data. Where now the experiments are a) more complex, i.e. represented by entire sequence of reactor core calculations, and b) indirect, i.e. measured core attributes are utilized to infer information about input data. For BWR simulation, we are interested in reducing the uncertainty in lattice-averaged few-group cross-sections and predicted core attributes uncertainties. The posterior probability distributions for the few-group cross-sections and core attributes follow Gaussian distributions since the core simulator behaves linearity over the range of the prior few-group cross-section uncertainties, thus can be fully described by posterior covariance matrices.

In the following, the uncertainty propagation equation, i.e. $\bar{\bar{\mathbf{C}}}_y = \bar{\bar{\boldsymbol{\Theta}}}\bar{\bar{\mathbf{C}}}_x\bar{\bar{\boldsymbol{\Theta}}}^{\mathbf{T}}$, for the linear relationship $\bar{\mathbf{y}} = \bar{\bar{\boldsymbol{\Theta}}}\bar{\mathbf{x}}$ is used to develop expressions for posterior covariance matrices $\bar{\bar{\tilde{\mathbf{C}}}}_z$, $\bar{\bar{\tilde{\mathbf{C}}}}_{FG}$, and $\bar{\bar{\tilde{\mathbf{C}}}}_{CA}$. After quite a bit of algebra, one can show that the few-group cross-section covariance matrix $\bar{\bar{\tilde{\mathbf{C}}}}_{FG}$ is given by:

$$\bar{\bar{\tilde{\mathbf{C}}}}_{FG} = \bar{\bar{\mathbf{U}}}_{FG}\bar{\bar{\tilde{\mathbf{C}}}}_z\bar{\bar{\mathbf{U}}}_{FG}^{T} \tag{22}$$

and the posterior covariance matrix $\bar{\bar{\tilde{\mathbf{C}}}}_z$ is given by:

$$\tilde{\tilde{\mathbf{C}}}_z = \tilde{\tilde{\mathbf{V}}}_A \tilde{\tilde{\mathbf{B}}}(\alpha^2)^{-1} \tilde{\tilde{\mathbf{B}}}(\alpha^4) \tilde{\tilde{\mathbf{B}}}(\alpha^2)^{-1} \tilde{\tilde{\mathbf{V}}}_A^T \tag{23}$$

where $\tilde{\tilde{\mathbf{B}}}(\eta)$ is a matrix operator:

$$\tilde{\tilde{\mathbf{B}}}(\eta) \equiv (\tilde{\tilde{\mathbf{\Sigma}}}_A^2 + \eta \tilde{\tilde{\mathbf{V}}}_A^T \tilde{\tilde{\mathbf{\Sigma}}}_{FG}^{-1} \tilde{\tilde{\mathbf{V}}}_A) \tag{24}$$

Finally, the posterior core attributes covariance matrix $\tilde{\tilde{\mathbf{C}}}_{CA}$ can be written as:

$$\tilde{\tilde{\mathbf{C}}}_{CA} = \tilde{\tilde{\mathbf{R}}}_c \tilde{\tilde{\mathbf{C}}}_z \tilde{\tilde{\mathbf{R}}}_c^T \tag{25}$$

Note that the rank of the above covariance matrices never exceeds ~10^2 - the effective rank of the multi-group covariance matrix. Therefore one never constructs the full covariance matrices as implied by the above equations; only their SVDs are computed and stored.

3. RESULTS

The methods described above were used to quantify core attributes' uncertainties for a BWR/3 reload core design with 540 fuel assembles and a cycle burnup of 16 GWD/MTU. The TRITON [11] lattice physics code developed at ORNL was used to calculate few-group cross-sections. The FORMOSA-B [12] core simulator, developed at North Carolina State University, was used as a core simulator to calculate core attributes of interest. Uncertainties in k_{eff} and nodal power were calculated for the 44GROUPANLCOV multi-group covariance library and the 44GROUPV5COV multi-group covariance library provided in the ORNL SCALE package. The 44GROUPV5COV library contained 600 different covariance matrices for 29 different isotopes. Key uncertainty contributors from this library include plutonium cross-sections and other minor actinide cross-sections for high burnup. The 44GROUPANLCOV library contains an additional 100 different covariance matrices for an additional 30 isotopes such as gadolinium, zirconium, and samarium cross-sections. The uncertainty was assumed to be zero for any cross-section not included in the libraries.

The k_{eff} standard deviation as a function of burnup is shown in Figure 1 using both covariance libraries. The standard deviation increases with burnup due to plutonium buildup as the core depletes. The k_{eff} standard deviation for the 44GROUPANLCOV library is ~40 pcm greater than that of the 44GROUPV5COV library which is to be expected since more sources of uncertainties in the multi-group cross-sections are now considered, i.e. the gadolinium cross-sections. As gadolinium depletes, the 44GROUPANLCOV standard deviation increases almost identically to the 44GROUPV5COV standard deviation due to plutonium buildup.

Standard deviations in relative nodal power are shown as a function of axial position at beginning of cycle (BOC), middle of cycle (MOC), and end of cycle (EOC) in Figure 2. The top three graphs show the standard deviation and the bottom three show the relative power profile for a fresh fuel assembly near the center of the core. The shape of the standard deviation is

complicated due to lattice type and history effects such as void, control rod, and burnup. The library difference is the largest at BOC where gadolinium is the key contributor to uncertainty.

An adaptive simulation experiment was conducted using the core attributes uncertainties given in Figures 1 and 2 to improve the fidelity of core simulator predictions by adjusting few-group cross-sections. Our goal is to use ESM based algorithms to adapt core simulators to real plant data. For now, a virtual approach is employed where a design basis core simulator, denoted DC, is adapted to a set of virtual core attributes, denoted VC. The virtual core attributes are generated by perturbing the few-group cross-sections in a statistically consistent manner with their prior uncertainties, specifically, the VC core attributes are calculated according to:

$$\bar{\mathbf{y}}^{\mathbf{VC}}_{CA(m)} = \boldsymbol{\Theta}(\bar{\mathbf{x}}_0 + \bar{\bar{\mathbf{U}}}_{FG}\bar{\zeta}) \tag{26}$$

where the columns of $\bar{\bar{\mathbf{U}}}_{FG}$ are the singular vectors of the prior few-group covariance matrix and $\bar{\zeta}$ denotes the perturbation size. In addition, the nodal powers were perturbed randomly by selecting them from Gaussian distribution with standard deviation of 4% which is representative of the in-core detectors signals' uncertainties. In the graphs that follow, AC denotes the adapted core solution. Figure 3 shows the k_{eff} differences before and after adaption using both the LANL and ORNL covariance libraries. The original difference <DC/VC> was 800 pcm at BOC and 1000 pcm at EOC. The differences after adaption are denoted <ANL-AC/VC> for the 44GROUPANLCOV library and <V5-AC/VC> for the 44GROUPV5COV library. The error in k_{eff} after adaption is nearly zero. Figure 4 plots the nodal power RMS errors as a function of burnup. The original nodal power error was 4.5-5.5%. The error decreased to 4.3% for the 44GROUPV5COV library and 4.1% for the 44GROUPANLCOV, consistent with the instrument noise level. Since the noise was simulated in this approach, we recalculate the RMS errors between the AC predictions and VC before the noise is applied, with <ANL-AC/VC*> and <V5-AC/VC*> representing the error in the AC nodal powers and the VC nodal powers before the noise is applied to the virtual core. The reduced RMS errors displayed indicate that the adaption acts as a powerful noise filter. The quality of the LANL-based adaption is better which is again expected due to the increased degrees of freedom available for the adaption.

The adapted solution results are used to generate posterior core attributes uncertainties. Posterior k_{eff} standard deviations are reported in Figure 5 and the posterior relative nodal power standard deviations are in Figure 6. The posterior uncertainty in k_{eff} for both libraries is of the order of 10 pcm, which is likely less than the uncertainty in k_{eff} due to modeling errors. The posterior uncertainty in nodal powers is less than 2%.

For this numerical experiment, the virtual core is created with the assumption that input data constitute the only source of uncertainties in the calculations. This is achieved by perturbing the reference cross-section along the singular vectors of the few-group prior covariance matrix, see Eq. 26. In reality, other sources of uncertainties are present, such as modeling uncertainties, and numerical errors. In these cases, the fidelity of the AC is expected to be lower since adaption can only correct for input data uncertainties. Previous work has illustrated that when both modeling and input data uncertainties are present, the adaption is shown to adjust a subset of input data outside the range of their prior uncertainties [2]. These data are associated with the models

introducing the modeling uncertainties. This helps provide some guidance to modelers on where further modeling development may be required.

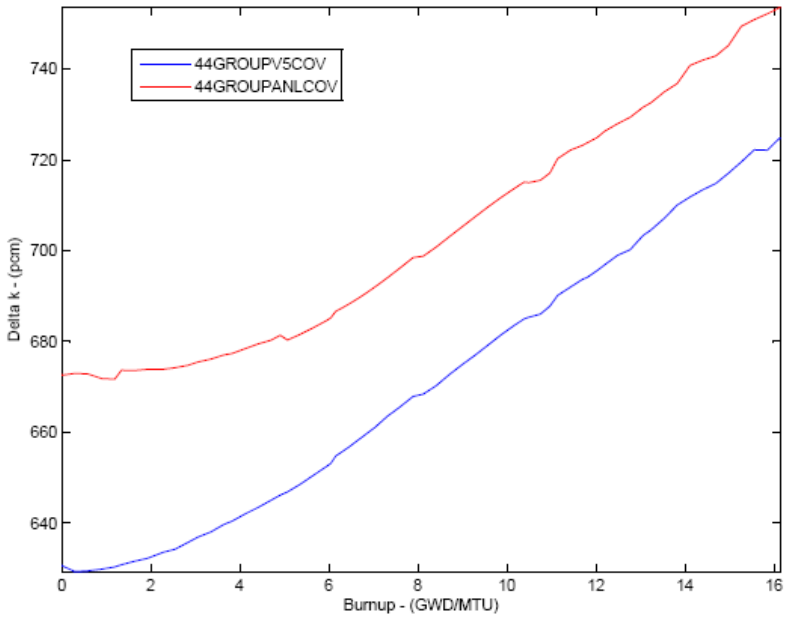

Figure 1. k_{eff} uncertainty as a function of burnup.

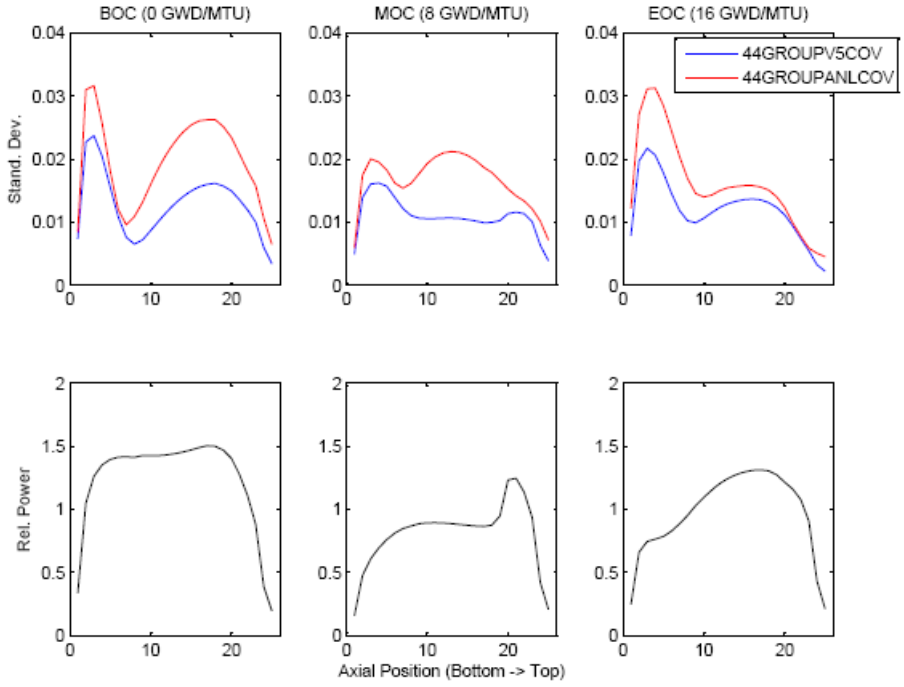

Figure 2. Nodal power uncertainty as a function of burnup.

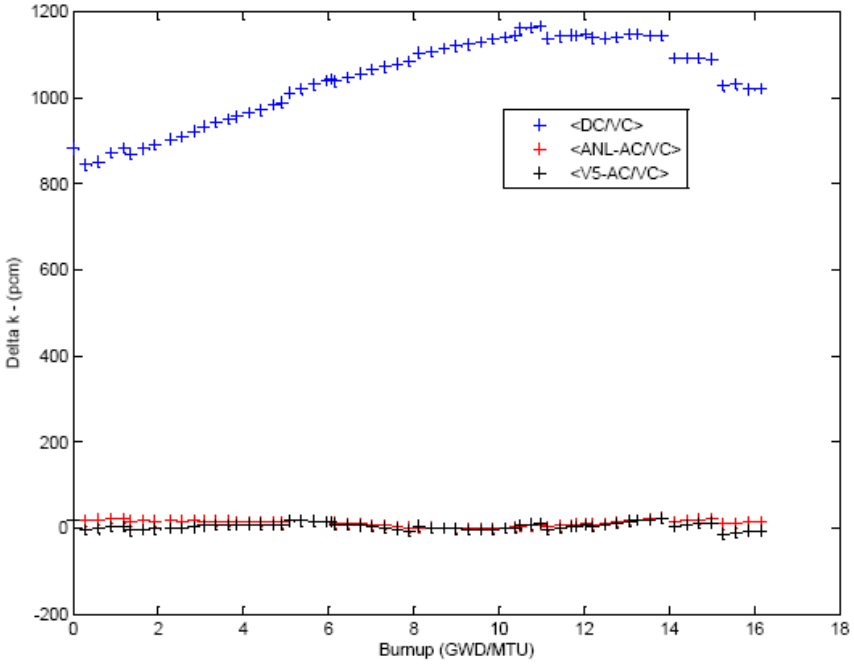

Figure 3. Reactivity difference as a function of burnup.

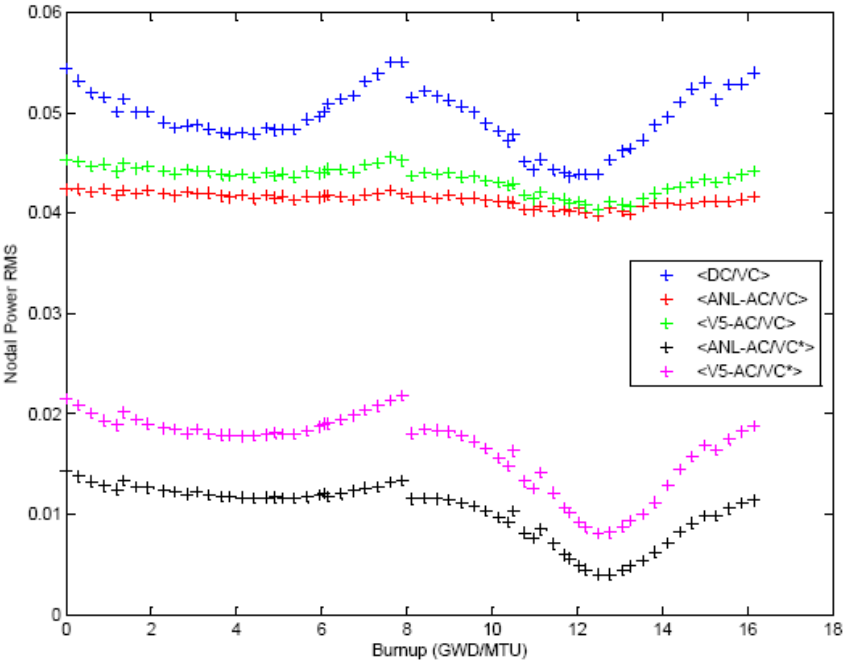

Figure 4. Nodal power RMS as a function of burnup.

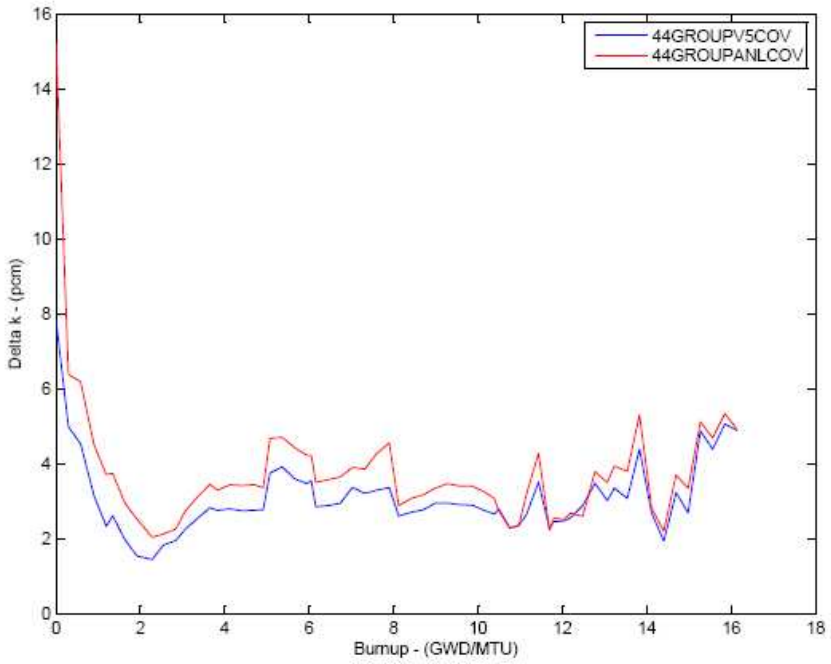

Figure 5 Posterior k_{eff} uncertainties.

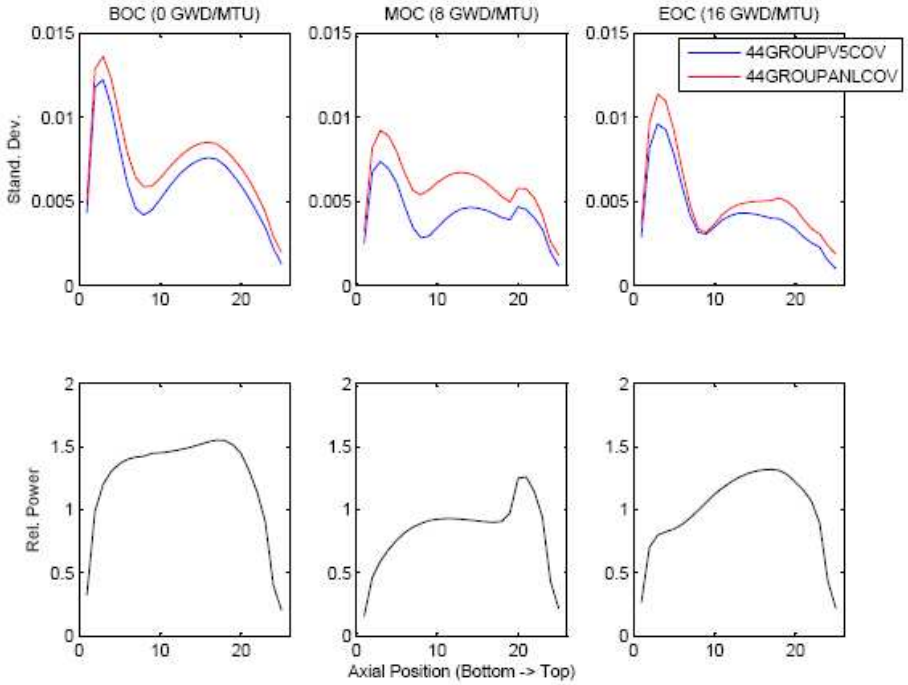

Figure 6 Posterior nodal power uncertainties.

4. CONCLUSIONS

Multi-group cross-section uncertainties have been propagated to uncertainties in core attributes, such as k_{eff} and nodal power, through the lattice physics calculations and core simulations in a computationally efficient manner based on the SVD of the multi-group covariance matrix. Adaptive core simulation algorithm have been proposed in which one can adjust for errors in the multitudes of data input to core simulators by utilizing an inverse theory approach that utilizes the discrepancies between measured and predicted core attributes. The key assumptions introduced are a) input data probability distributions can be well represented by normal Gaussian distribution, b) reactor calculations, including lattice physics and core simulations, behave linearly within the range of input data uncertainty, and c) the rank of the associated sensitivity matrices are remarkably low such that few forward calculations are required to evaluate the required matrices for both the uncertainty and the adaptive simulation application. The 44GROUPANLCOV library provided better adaption than the 44GROUPV5COV library due to larger number of degrees of freedom. Current work focuses on the adaption of the multi-group cross-sections rather than few-group cross-sections. This adaption is expected to be more robust since the cross-section adjustments will no longer depend on the specific lattice design and/or even core design; thus eliminating the need to repeat the adaption when a new fuel design is introduced.

REFERENCES

1. H. S. Abdel-Khalik and P. J. Turinsky, "Evaluation of Core Attributes Uncertainties due to Input Data Uncertainties," Transactions of the American Nuclear Society, **92**, San Diego, (2005).
2. H. S. Abdel-Khalik, "Adaptive Core Simulation," Ph.D. Dissertation, North Carolina State University, December (2004).
3. Y. Ronen, *Uncertainty Analysis*, CRC Press (1988).
4. C. T. Kelley, *Iterative Methods for Linear and Nonlinear Equations*, Society for Industrial and Applied Mathematics, Philadelphia USA (1995).
5. "SCALE: A Modular Code System for Performing Standardized Computer Analyses for Licensing and Evaluation," NUREG/CR-0200, ORNL/NUREG/CSD-2/R6 (2000).
6. M. E. Dunn, "PUFF-III: A Code for Processing ENDF Uncertainty Data Into Multi-group Covariance Matrices," NUREG/CR-6650, ORNL/TM-1999/235 (2000).
7. J. Hadamard, *Bull. University Princeton*, 13, p. 49 (1902).
8. A. N. Tikhonov, "Regularization of incorrectly posed problems," *Soviet Mathematics Doklady*, 4, 1624 (1963).
9. H. W. Engl and W. Grever, "Using the L-Curve for determining optimal regularization parameters," *Numerische Mathematik*, **69**, p. 25, (1994).
10. A. Tarantola, *Inverse Problem Theory and Methods for Model Parameter Estimation*, Society for Industrial and Applied Mathematics, Philadelphia USA (2005).
11. M. D. DeHart, "TRITON: A Two Dimensional Depletion Sequence for Characterization of Spent Nuclear Fuel," NUREG-0200, ORNL/NUREG/CSD-2/R7, DRAFT (2004).
12. B. R. Moore, P. J. Turinsky and A. A. Karve, "FORMOSA-B: A Boiling Water Reactor In-core Fuel Management Optimization Package," *Nuclear Technology*, **126**, p. 153 (1999).